SCIENCE CHINA
Chemistry

•ARTICLES•

May 2022 Vol.65 No.5: 979–988
https://doi.org/10.1007/s11426-021-1199-6

A near-infrared plasma membrane-specific AIE probe for fluorescence lifetime imaging of phagocytosis

Ming-Yu Wu[1,2], Jong-Kai Leung[1], Chuen Kam[1], Tsu Yu Chou[1], Jia-Li Wang[2], Xueqian Zhao[1], Shun Feng[2] & Sijie Chen[1*]

[1]*Ming Wai Lau Centre for Reparative Medicine, Karolinska Institutet, Hong Kong, China;*
[2]*Sichuan Engineering Research Center for Biomimetic Synthesis of Natural Drugs, School of Life Science and Engineering, Southwest Jiaotong University, Chengdu 610031, China*

Received October 6, 2021; accepted January 19, 2022; published online March 17, 2022

Phagocytosis is a biological process that plays a key role in host defense and tissue homeostasis. Efficient approaches for real-time imaging of phagocytosis are highly desired but limited. Herein, an AIE-active near-infrared fluorescent probe, named **TBTCP**, was developed for fluorescence lifetime imaging of phagocytosis. **TBTCP** could selectively label the cell plasma membrane with fast staining, wash-free process, high signal-to-background ratio, and excellent photostability. Cellular membrane statuses under different osmolarities as well as macrophage phagocytosis of bacteria or large silica particles in early stages could be reported by the fluorescence lifetime changes of **TBTCP**. Compared with current fluorescence imaging methods, which target the bioenvironmental changes in the late phagocytosis stage, this approach detects the changes in the cell membrane, thus giving a faster response to phagocytosis. This article provides a functional tool to report the phagocytic dynamics of macrophages which may greatly contribute to the studies of phagocytic function-related diseases.

fluorescence lifetime imaging, phagocytosis, plasma membrane, aggregation-induced emission, near-infrared

Citation: Wu MY, Leung JK, Kam C, Chou TY, Wang JL, Zhao X, Feng S, Chen S. A near-infrared plasma membrane-specific AIE probe for fluorescence lifetime imaging of phagocytosis. *Sci China Chem*, 2022, 65: 979–988, https://doi.org/10.1007/s11426-021-1199-6

1 Introduction

Phagocytosis, a fundamental cellular process that cells recognize and internalize extracellular substances, is an essential mechanism in the innate immunity of multicellular organisms [1,2]. Phagocytes, which are a group of specialized cells including macrophages, neutrophils, dendritic cells, *etc.*, are responsible for the removal of microorganisms and foreign particles [3]. Phagocytosis is also crucial for the clearance of apoptotic cells during normal tissue homeostasis and remodeling by non-professional phagocytes [4]. Therefore, phagocytic signaling and machinery have been proposed as new targets for disease treatment such as cancer immunotherapy [5]. In general, phagocytosis involves four major steps: (1) recognition of targets, (2) activation of phagocytic signaling pathways, (3) engulfment of targets, and (4) phagosome maturation [6]. This process is very fast that can finish within minutes [7]. Real-time imaging phagocytosis that reveals the subtleties of phagocytic dynamics is of great importance for cellular phagocytic studies and directly benefits the development of methods for diagnosis and treatment of phagocytic function-related diseases [8]. Fluorescence imaging is an indispensable technique for visualizing biological molecules and structures, tracking physiological and pathological processes, as well as diagnosing diseases in complex biological systems [9]. For phagocytosis imaging, the observation of cell internalization of fluorescently labeled targets is straightforward but tricky since

*Corresponding author (email: sijie.chen@ki.se)

sometimes it is difficult to distinguish if a target is inside, beside, atop, or outside of the cell [10]. Based on the diverse biological processes induced by phagocytosis, a variety of reactivity-based fluorescent probes, such as probes for pH, reactive oxygen species, reactive nitrogen species, and enzymes, are developed to image the activated phagocytes [11]. Most of these probes are based on fluorescence intensities, which can be easily interfered by a variety of factors such as local probe concentrations. More importantly, these reactivity-based fluorescent probes mainly target the intracellular activities in the late phagocytosis, which require a time-dependent accumulation of reactive substances to high levels. Real-time monitoring of phagocytosis at a high time resolution and imaging of phagocytosis at early stages with a good sensitivity is therefore difficult to achieve. Fluorescence lifetime imaging, in which the signal contrast is based on the fluorescence lifetime of the fluorophores rather than their emission intensities, has attracted increasing attention [12]. The fluorescence lifetime is independent of fluorophore concentration, fluorescence absorption by surrounding background, photobleaching, and excitation/emission intensities, therefore enabling it to be more robust than intensity-based fluorescence measurements [13]. Furthermore, the fluorescence lifetime depends on a wealth of cellular microenvironment, making it the choice of techniques for functional imaging of many kinds [14–19]. Since the concept of aggregation-induced emission (AIE) was proposed, it has emerged as a group of excellent candidates for bioimaging [20–26]. AIE luminogens show weak emission in dilute solution but emit strong fluorescence in the aggregated state or when binding with subcellular organelles or biomacromolecules. The restriction of intramolecular motions favors fluorescence lifetime imaging ascribed to the high sensitivity of AIE fluorophores towards the microenvironment of the target [27]. However, there are few studies using AIE fluorescent probes in fluorescence lifetime imaging, and none of these probes are applied in the study of phagocytosis [28–30].

During phagocytosis, especially in the early stages, the plasma membrane is considered an essential structure involved in the process. Phagocytes rely on several pathogen recognition receptors on the plasma membrane to recognize and distinguish foreign pathogen-associated molecular patterns as their targets. When phagocytes attempt to uptake microbial pathogens from the extracellular matrix, extension and remodeling of the plasma membrane into pseudopods contribute to the engulfment of those targets [1,6]. Interestingly, other researchers discover that phospholipid redistribution in the plasma membrane during phagocytosis leads to changes in lipid order and dynamics [31–34]. In other words, the plasma membrane plays a pivotal role in mediating engulfment through membrane remodeling during early phagocytosis, and this characteristic allows it to be a direct monitoring target of phagocytosis [35]. If such changes of the plasma membrane can be monitored, presumably, it will be feasible to study phagocyte response when interacting with foreign particles. Although many plasma membrane-targeting probes have been developed and some of them are AIE-active [36–43], these probes were seldomly used for sensing phagocytosis. Zhang *et al*. [44] developed a plasma membrane-targeting probe for real-time monitoring of phagocytosis. However, it was only used for the imaging of the plasma membrane morphology. A fluorescent probe that can be used for both imaging and sensing the phagocytosis process would be highly desired. Based on this postulation, here we developed a novel plasma membrane targeting fluorescent AIE probe named **TBTCP** to monitor phagocytosis. **TBTCP** showed AIE properties with near-infrared (NIR) emission. It specifically labeled the plasma membrane in living cells with excellent photostability. Compared with the commercial plasma membrane probes, **TBTCP** showed a high signal-to-background ratio with fast staining (30 s) and a wash-free process. Furthermore, through the advanced fluorescence lifetime imaging microscopy (FLIM), **TBTCP** could be used to sense the cell membrane topographic changes induced by osmolarity variations and study the early phagocytosis in macrophages toward different kinds of bacteria and different sizes of silica particles in real-time.

2 Experimental

2.1 Materials and general instruments

All chemical reagents were obtained from J&K Scientific (China) and were used without further purification. CCK-8 kit was purchased from MedChemExpress. Dulbecco's modified eagle's medium (DMEM), RPMI 1640, Trypsin-EDTA, fetal bovine serum (FBS), penicillin, and streptomycin were purchased from Gibco (USA). Phosphate buffered saline (PBS) was purchased from Invitrogen (USA). CellMask™ Green and Vybrant DiO were purchased from Thermo Fisher Scientific (USA). TPE-2BA was available from AIEgen Biotech Co., Ltd. (USA). All the solvents for optical spectroscopic studies were high performance liquid chromatography (HPLC) or spectroscopic grade. Thin layer chromatography (TLC) analyses were performed on silica gel GF 254. Column chromatography purification was carried out on silica gel (200–300 mesh). Nuclear magnetic resonance (NMR) spectra were recorded using Bruker AMX-400 or AMX-600 (Germany). Chemical shifts were given in ppm relative to the internal reference tetramethyl silane (TMS), $CDCl_3$ or dimethyl sulfoxide (DMSO)-d_6 as the internal standard. The following abbreviations were used in ^{1}H NMR: s = singlet; d = doublet; t = triplet; q = quartet; m = multiplet. High resolution mass spectra were recorded on a

Bruker Daltonics Bio TOF mass spectrometer. Fluorescence spectra were obtained using a Horiba Duetta spectrofluorimeter (USA) with a 10 mm quartz cuvette. UV-Vis absorption spectra were recorded on a Hitachi PharmaSpec UV-1900 UV-Visible spectrophotometer (Japan). The average particle size of the samples was recorded on a Brookhaven Zeta Plus potential analyzer at 25 °C. The fluorescence distribution was monitored by the Zeiss LSM 880 Confocal Laser Scanning Microscope (Germany).

2.2 Synthesis and characterization of TBTCP

The synthetic procedure of **TBTCP** is illustrated in Scheme 1 with the detailed procedure as follows.

2.2.1 Synthesis of BCN

To a 50 mL MeOH solution of 2-(5-bromothiophen-2-yl) acetonitrile (5.05 g, 25 mmol), 5-bromothiophene-2-carbaldehyde (4.775 g, 25 mmol) was added 1.3 g sodium methoxide (25 mmol). The reaction mixture was stirred at room temperature (RT) for 24 h, and the precipitate was filtrated. The crude product was purified by silica gel column chromatography using methylene dichloride as an eluent. The product was obtained as a yellow solid (5.06 g). Yield: 54%.

2.2.2 Synthesis of BCN-Py

Into a 100 mL two-necked round bottom flask equipped with a condenser were added BCN (375 mg, 1.0 mmol), K_2CO_3 (1380 mg, 10 mmol) and $Pd(PPh_3)_4$ (23 mg, 2% mmol) in 30 mL tetrahydrofuran (THF) and 6 mL water under N_2. After the mixture was heated to reflux, pyridin-4-ylboronic acid (123 mg, 1.0 mmol) in 20 mL THF was added dropwise more than 1 h under N_2 and the mixture was then stirred under reflux overnight. After cooling to room temperature, the mixture was extracted with dichloromethane (DCM) three times. The organic phase was collected, washed with saturated salt solution and dried over anhydrous sodium sulfate. After solvent evaporation, the mixture was purified by silica gel column chromatography using DCM/ethyl acetate (V:V = 20:1) as eluent to obtain 261 mg yellow solid crude product without further purification (about 70% yield).

2.2.3 Synthesis of BCN-Py-TPA

Into a 100 mL two-necked round bottom flask equipped with a condenser were added BCN-Py (90 mg, 0.24 mmol), (4-(diphenylamino)phenyl)boronic acid (90.6 mg, 0.31 mmol), K_2CO_3 (333 mg, 2.4 mmol) and 5.5 mg $Pd(PPh_3)_4$ (0.48% mmol) in 20 mL THF and 3 mL water under N_2. The mixture was stirred and heated to reflux overnight. After cooling to room temperature, the mixture was extracted with DCM three times. The organic phase was collected, washed with saturated salt solution and dried over anhydrous sodium sulfate. After solvent evaporation, the crude product was purified by silica gel column chromatography unsing DCM as eluent to furnish 117.4 mg red solid, yield: 91%.

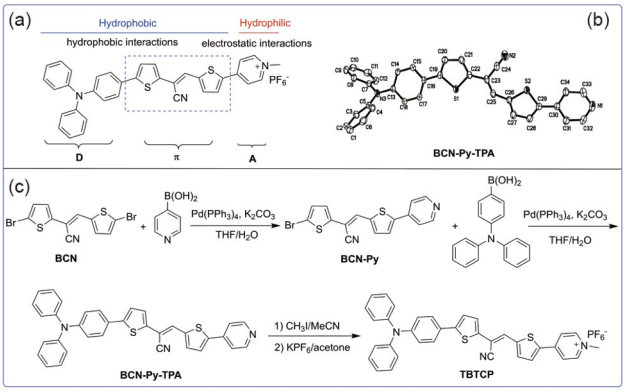

Scheme 1 (a) The chemical structure, schematic illustration of **TBTCP** structural characteristics, and its interaction with membrane structure. (b) The crystal structure of BCN-Py-TPA. (c) Synthetic route to **TBTCP** (color online).

^{1}H NMR (600 MHz, DMSO-d_6), δ. 8.63 (d, 2H, J = 6.6 Hz), 8.03 (s, 1H), 7.94 (d, 1H, J = 3.6 Hz), 7.80 (d, 1H, J = 4.2 Hz), 7.71 (dd, 2H, J = 1.8 Hz, J = 4.8 Hz), 7.60 (dd, 2H, J = 1.8 Hz, J = 6.6 Hz), 7.47 (d, 1H, J = 4.2 Hz), 7.41 (d, 1H, J = 3.6 Hz), 7.35 (t, 4H, J = 7.8 Hz), 7.12–7.07 (m, 6H), 6.98 (dd, 2H, J = 1.8 Hz, J = 6.6 Hz).

^{13}C NMR (150 MHz, DMSO-d_6), δ. 150.6, 147.6, 146.7, 144.7, 144.1, 139.5, 138.6, 136.1, 135.8, 131.8, 129.7, 129.2, 128.3, 127.3, 126.6, 126.3, 124.7, 124.6, 123.9, 123.8, 122.4, 119.7, 116.6, 102.1.

HRMS (ESI): m/z $[M + H]^+$ calcd. for $C_{34}H_{24}N_3S_2$: 538.1406; found 538.1429.

*2.2.4 Synthesis of **TBTCP***

Into a 100 mL round bottom flask were added 107.5 mg BCN-Py-TPA (0.2 mmol) and 15 mL acetonitrile. Iodomenthane (0.3 mL) was then added and the mixture was heated to reflux for 12 h. After cooling to RT, the mixture was evaporated under reduced pressure. The dark red solid was dissolved in 10 mL acetone and mixed with saturated KPF_6 solution in 5 mL acetone. After stirring for 1 h, acetone was removed. The crude products were purified by silica gel column chromatography using DCM/MeOH (V:V = 100:5) as eluent to dark red solid with 95% yield.

^{1}H NMR (600 MHz, DMSO-d_6) δ. 8.89 (d, 2H, J = 7.2 Hz), 8.39 (d, 2H, J = 7.2 Hz), 8.30 (d, 1H, J = 3.6 Hz), 8.08 (s, 1H), 7.89 (d, 1H, J = 4.2 Hz), 7.60 (dd, 2H, J = 2.4 Hz, J = 7.2 Hz), 7.48 (dd, 2H, J = 4.2 Hz, J = 14.8 Hz), 7.36 (dt, 4H, J = 1.8 Hz, J = 8.4 Hz), 7.12 (dt, 2H, J = 1.2 Hz, J = 7.8 Hz), 7.08 (dd, 4H, J = 1.2 Hz, J = 9.0 Hz), 6.98 (d, 2H, J = 9.0 Hz), 4.27 (s, 3H).

^{13}C NMR (150 MHz, DMSO-d_6) δ. 147.8, 146.6, 146.5, 145.7, 143.2, 139.6, 136.0, 135.7, 132.2, 130.8, 129.8, 129.4, 126.6, 126.0, 124.9, 124.8, 124.1, 123.9, 122.4, 122.2, 116.3, 104.5, 47.0.

HRMS (ESI): *m*/*z* $[M\text{-}PF_6^-]^+$ calcd. for $C_{35}H_{26}N_3S_2$: 552.1563; found 552.1546.

2.3 Cell culture

HeLa, HEK-293T, MDA-MB-231, MCF-7, RAW 264.7, and NIH-3T3 cells were maintained in DMEM supplemented with 10% FBS, 100 units/mL of penicillin, and 100 μg/mL of streptomycin in a 5% CO_2 humidity incubator at 37 °C. HepG2 cells were maintained in RPMI 1640 medium supplemented with 10% FBS, 100 units/mL of penicillin, and 100 μg/mL of streptomycin in a 5% CO_2 humidity incubator at 37 °C. Once the cells (except RAW 264.7 cells) reached 80%–90% confluence, they were dissociated into single cells with 0.05% Trypsin-EDTA at 37 °C for 5 min and passaged at a ratio of 1:6–1:19 in a new cell culture dish. On the other hand, RAW 264.7 cells were scrapped for subculture when the confluence reached 60%–70% and passaged at a ratio of 1:5–1:10 in a new T75 cell culture flask. In corresponding experiments, HeLa cells were further treated with solutions of different osmolarities or a bacterial culture *E. coli*. The NaCl aqueous solution was used for preparing hypertonic (1.215 osm), isotonic (0.308 osm), and hypotonic (0.104 osm) solutions in DMEM. RAW 264.7 cells were treated with different bacterial strains, lipopolysaccharides (LPS) from *E. coli* O111:B4 (Sigma-Aldrich, USA), or different sizes of silica particles (in 5% weight fraction, diluted with DMEM in 1:8) (Sigma-Aldrich).

2.4 Bacteria culture, staining, and imaging

E. coli K-12 strain, *B. subtilis*, and *S. epidermidis* were grown in LB liquid culture medium at 37 °C for overnight. The concentration of bacteria was determined by measuring the optical density at 600 nm (OD_{600}) and calculated using OD_{600} calculator (Agilent). 1×10^9 of bacteria were further collected and harvested by centrifuging at 8,000×*g* for 3 min. After discarding the supernatant, bacteria were washed twice with Milli-Q water. For the TPE-2BA staining, the bacteria were fixed with 75% ethanol for 20 min at room temperature, followed by rinsing with Milli-Q water twice to remove the ethanol and resuspensing in Milli-Q water. After the fixation, fixed bacteria were stained with 100 μM TPE-2BA for 2 h and then washed with Milli-Q water three times.

2.5 MTT assay for the cell cytotoxicity

The cytotoxicity of **TBTCP** in HeLa cells was determined by the standard 3-(4,5-dimethylthiazol-2-yl)-2,5-diphenyl-2*H*-tetrazolium bromide (MTT) assay. HeLa cells were seeded at a density of 7×10^3 cells per well in 96-well black plates with 100 μL of culture medium and cultured overnight to reach 70%–80% confluence. After that, the medium was replaced with 100 μL of fresh medium containing different concentrations of probes (0, 0.25, 0.5, 1.0, 2.5, 5.0, 7.5, or 10 μM) and DMSO was used as vehicle control. After 24 h of incubation, 10 μL of 12 mM MTT stock solution (Sigma-Aldrich) mixed with 90 μL of PBS was added to each well for an additional 4 h of incubation. The absorbance was measured at 570 nm using a SpectraMax M2 microplate reader (Molecular Devices). Cell viability (%) was calculated as: (OD_{570} sample/OD_{570} control) × 100%.

2.6 Confocal laser scanning microscopy imaging

Cells were stained with 2.5 μM DTTPB for 10 min at 37 °C. After the incubation, the cells were washed with dulbecco's PBS (DPBS) three times. Confocal imaging was performed using the Zeiss LSM 880 laser scanning confocal microscope equipped with a Plan-Apochromat 63×/1.4 NA oil objective lens, a photo-multiplier tube, and a Gallium arsenide phosphide detector driven by the ZEN software (Carl Zeiss). The 514 nm laser and 620–720 nm emission filter were used for **TBTCP**. The 488 nm laser and 500–600 nm emission filter were used for CellMask™ Green and Vybrant™ DiO. The 405 nm laser and 410–480 nm emission filter were used for TPE-2BA. Digital images were acquired with ZEN software (ZEN 2.5 lite) in grayscale and pseudocolored.

2.7 Fluorescence lifetime imaging

The RAW 264.7 cells were incubated with 2.5 μM **TBTCP** for 30 min and then washed with PBS. Subsequently, the cells were treated with different osmolarities solutions, different kinds of bacteria, the culture supernatant, different-sized silica particles. The fluorescence lifetime imaging was recorded by the microscope after the treatment at 37 °C for 5 min. For LPS-induced pro-inflammatory response, RAW 264.7 cells were first treated by LPS for 24 h and then stained with **TBTCP**. The fluorescence lifetime decays of **TBTCP** in plasma membrane were measured by the Nikon Eclipse Ti2 Inverted Microscope (Nikon) with a pco.flim system and frequency domain FLIM camera (PCO) with 514 nm laser and 520 nm long pass emission filter. The fluorescence lifetime mapping of **TBTCP** in cells was presented as pseudocolor images and was further processed by the NIS-Elements AR imaging software (Nikon) or Fiji/Image J (NIH).

2.8 Data and statistical analysis

The Pearson correlation coefficient was obtained using the NIS-Element AR imaging software. For the statistical analysis, experiments were performed at least three times, and data were presented as mean ± standard deviation (SD) or mean ± standard error of mean (SEM). Statistical sig-

nificance was determined by the *P* value in the Student's *t*-test. Signal-to-background ratio was defined as (mean fluorescence signal)/(mean background signal).

3 Results and discussion

3.1 Molecule design and synthesis

Our molecular design of the probe was mainly based on three considerations: NIR emission, plasma membrane targeting, and non-planar conformation for AIE attribute. Generally, intramolecular charge transfer (ICT) with D-π-A structures, which results in lower electronic bandgaps, is an efficient and widely used strategy to design NIR probes [45]. To target the plasma membrane, the amphiphilic structure is preferred to mimic the structure of phospholipids in the membrane [36]. α,β-Diaryl-acrylonitrile was chosen as the AIE fluorescent skeleton since the cyano group has steric effects on the diarylethene backbone. It is significantly nonplanar with a low rotational energy barrier which is highly favorable for the construction of AIE fluorescent probes [46]. Strong electron-donating group triphenylamine and strong electron-withdrawing group pyridinium are D and A, respectively, and the thiophene serves as the good electron donor and π-bridge. The donor and π-bridge of **TBTCP** are hydrophobic, which will be embedded into the non-polar hydrocarbon chains of phospholipids through hydrophobic interactions. The acceptor pyridinium salt with a positive charge is hydrophilic, which aligns on the surface of lipid bilayers and binds to the negatively charged phosphate group of phospholipids through strong electrostatic interactions. These together will facilitate its targetability to plasma membranes (Scheme 1a).

As depicted in Scheme 1c, **TBTCP** was synthesized by a three-step reaction with reasonable yields. The first two steps regionally selective Suzuki coupling reaction proceeded separately, which generated BCN-Py-TPA. Then, BCN-Py-TPA reacted with methyl iodide and KPF_6 to acquire **TBTCP**. The intermediate and final products were characterized by ^{1}H NMR, ^{13}C NMR, and high resolution mass spectrometry (HRMS) (Supporting Information online). The molecular structure and absolute configuration of the BCN-Py-TPA were further confirmed by X-ray single-crystal diffraction (Scheme 1b, and Supporting Information online).

3.2 Photophysical properties

The optical properties of **TBTCP** were investigated by photoluminescence spectrometry. It showed the maximum absorption peak at 515 nm in dimethyl sulfoxide and maximum emission peak at 821 nm in the solid state with a 306 nm Stokes shift (Figure 1a). We then used mixed solvent (DMSO/toluene) with different toluene (PhMe) fractions as the solvent system to evaluate the AIE properties. As depicted in Figure 1b, **TBTCP** showed barely any emission in pure DMSO solution with a quantum yield (QY) of 0.11% and very weak emission when PhMe fraction (f_T) was below 80% (Figure 1b). Further increasing f_T beyond 80% led to aggregate formation with an enhanced and blue-shifted emission. The fluorescence intensity of **TBTCP** in 99.9% PhMe solution was 495.8 folds higher than that in pure DMSO and the QY increased to 10.3% (Figure 1c). The aggregate formation was confirmed by dynamic light scattering with an average size of 116.4 nm (Figure 1d). As a result, these data affirmatively indicate the typical AIE properties of **TBTCP**.

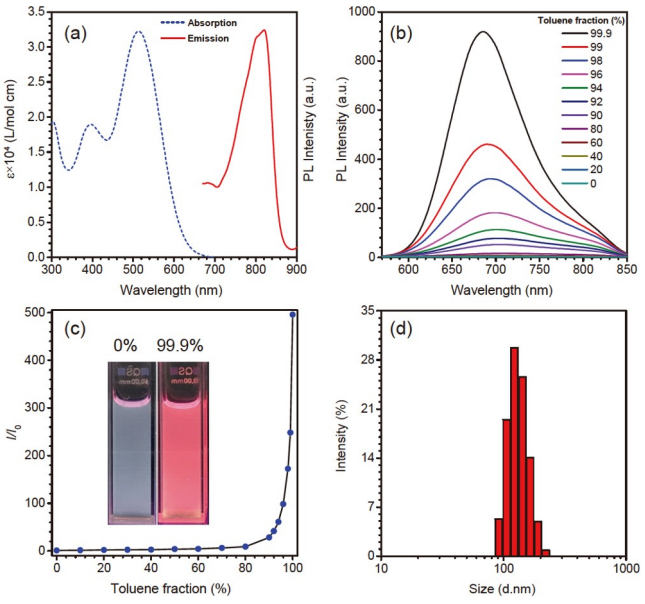

Figure 1 Photophysical properties of **TBTCP**. (a) The molar absorption coefficient of **TBTCP** in DMSO and its emission spectrum in the solid state. (b) Photoluminescence spectra of **TBTCP** (10 μM) in the mixtures of DMSO and toluene (PhMe) with different PhMe fractions. Excitation: 505 nm. (c) The plot of the relative emission intensity of **TBTCP** *versus* PhMe fractions. I_0 and I are the peak values of photoluminescence intensities of **TBTCP** in DMSO and DMSO/PhMe mixtures, respectively. Inset: fluorescence images of **TBTCP** in DMSO solution (0% PhMe) and aggregated state (99.9% PhMe) with 365 nm excitation. (d) Size distribution of **TBTCP** in the mixture of DMSO/PhMe with 99.9% PhMe content (color online).

The optical properties of **TBTCP** in different lipids were also investigated. Due to the strong twisted intramolecular charge transfer (TICT) effect, **TBTCP** had no emission in highly polar solvents such as water, MeOH, and glycerol. The very low quantum yield in water (0.01%) indicated the "off" state of **TBTCP** in the aqueous environment, and thus it had great potential to serve as a "light-up" probe for bioimaging with minimal background interference. Once the phospholipid was added, the fluorescence intensity showed a significant increase with maximal emission blue-shifted (Figure S1, Supporting Information online). The fluorescence quantum yields of **TBTCP** were 10.3% in aggregated

state, 23.5% in unsaturated lipid, 1,2-dioleoyl-sn-glycero-3-phosphocholine (DOPC) and rose to 26.6% in DOPC-cholesterol (4:1, DC). We then investigated the lifetime of the **TBTCP** in different lipid, aggregated state, and solid state. As shown in Figure S2, the fluorescence lifetime of **TBTCP** was prolonged when the lipid changed from unsaturated phospholipids to unsaturated phospholipids with cholesterol and further increased in saturated phospholipids. The fluorescence lifetimes were 0.7 ns (solid), 1.0 ns (aggregate, toluene), 2.3 ns (DOPC), 3.0 ns (DC) and 3.2 ns (saturated phospholipid, 1,2-dimyristoyl-sn-glycero-3-phosphate, 14-0 PA). These results suggest that the lipid is an important factor that affects the fluorescence intensity and lifetime of **TBTCP**.

3.3 Fluorescence imaging of plasma membrane

Ascribed to the typical AIE properties and NIR emission, several experiments were conducted to investigate the bioimaging performance of **TBTCP**. Before we applied **TBTCP** in cell imaging, cytotoxicity was tested by evaluating cell viability using standard MTT assays (Figures S3, S4). The data showed that viability of HeLa cells and RAW 264.7 cells were more than 95% after 24 h of incubation with 5 μM **TBTCP**, and 88.5% of cells survived in the presence of 10 μM **TBTCP**. These data demonstrated the good biocompatibility of **TBTCP**. Then, the cell imaging study was performed in living HeLa cells. After incubating HeLa cells with 2.5 μM **TBTCP** for 10 min at room temperature, **TBTCP** selectively accumulated in the cell membrane and emitted strong red fluorescence. The colocalization experiment was also carried out using the commercially available cell membrane selective probe CellMask™ Green as a reference. In this experiment, HeLa cells were incubated with 2 μM CellMask™ Green and 2.5 μM **TBTCP** for 10 min at 37 °C followed by confocal imaging. As shown in Figure 2a, the red fluorescence signal of **TBTCP** well overlapped with the green fluorescence signal of CellMask™ Green and the Pearson correlation coefficient (R_r) was 0.857 (Figure S5), indicating the good selectivity of **TBTCP** to the cell membrane. As shown in Figure 2a, HeLa cells stained with CellMask™ Green showed a lot of puncta in the cytoplasm, yet the cells stained with **TBTCP** exhibited explicit fluorescence signals on the cell membrane region. It suggested that **TBTCP** had a better cell membrane selectivity when compared with CellMask™ Green. Generally, many commercial plasma membrane probes can be easily internalized by the cells and long staining procedures often cause nonspecific staining of other subcellular compartments [40]. Therefore, we evaluated the influence of the incubation length of **TBTCP** on the cell staining performance. As shown in Figure S6, the cell membrane could be labeled after incubated with 5 μM **TBTCP** for 2 min without the washing

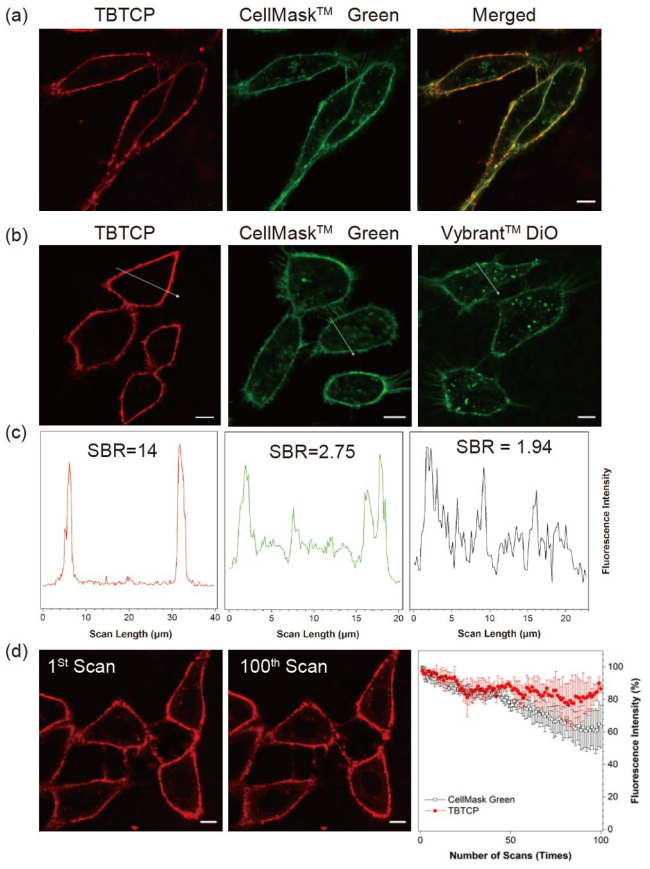

Figure 2 The **TBTCP**-labeled plasma membrane of HeLa cells under confocal imaging. (a) Fluorescence imaging of HeLa cells stained with **TBTCP** (red) and CellMask™ Green (green). Scale bar: 10 μm. (b) Confocal fluorescence images of HeLa cells stained with **TBTCP** without PBS washing or stained with CellMask™ Green or Vybrant DiO with PBS washing. Scale bars: 10 μm. (c) Corresponding fluorescence intensity profiles of the marked white lines in panel B. (d) Photostability test of **TBTCP** labeling in the plasma membrane of HeLa cells. The images were acquired in the 1st and the 100th scan. The fluorescence intensity of **TBTCP** (red solid Circle) or CellMask™ Green (black open square) was quantified in 100 times of scanning by a confocal laser scanning microscope. Scale bars: 10 μm (color online).

step. There were no obvious changes in both fluorescence intensity and cell membrane selectivity along with the reduction of staining time from 2 min to 30 s, indicating that **TBTCP** can be used for ultrafast labeling of the cell membrane with a wash-free process. Then, we measured the signal-to-background ratio of **TBTCP** and compared it with two widely used fluorescence dyes for the cell membrane. As illustrated in Figure 2b, c, in cells stained with a wash-free process, **TBTCP** exhibited strong fluorescence signals in the cell membrane and the signal-to-background ratio was as high as 14. The signal-to-background ratios of CellMask™ Green and Vybrant™ DiO were only 2.75 and 1.94, respectively, even with the washing step.

Subsequently, the photostability of **TBTCP** and CellMask™ Green was evaluated with continuous excitation and sequential scanning with a confocal microscope (Figure 2d).

The result showed that CellMask™ Green lost about 40% fluorescence within 100 scans, while **TBTCP** remained 86% of its original fluorescence intensity in comparison, indicating a better photostability of **TBTCP**. Additionally, the application of **TBTCP** in plasma membrane imaging in different types of cells was investigated. As shown in Figure S7, **TBTCP** demonstrated high selectivity to the cell membrane in different cell types such as hepatocellular carcinoma (HepG2 cells), breast cancer cells (MDA-MB-231 and MCF-7), human embryonic kidney cells (HEK-293T), mouse macrophages (RAW 264.7), and mouse embryo fibroblast cells (NIH-3T3).

3.4 TBTCP reports plasma membrane topographic changes under different osmolarities

Due to the superior properties of **TBTCP** in fluorescence imaging of plasma membrane, we further applied **TBTCP** in fluorescence lifetime imaging and tested its sensitivity to environmental changes. Osmotic shock is a general approach to alter the membrane tension, which remodels the plasma membrane in response to extracellular challenges [15]. Under the FLIM, it showed that the mean fluorescence lifetime of **TBTCP** on the cell membrane was 3.443 ns when cells were incubated in isotonic solutions, while its fluorescence lifetime rapidly changed under hypotonic or hypertonic shocks (Figure 3 and Figure S8). We observed longer mean fluorescence lifetimes (3.482 ns) under hypotonic shocks but shorter mean fluorescence lifetimes (3.354 ns) under hypertonic shocks. These results suggested that the fluorescence lifetime of **TBTCP** is sensitive to the environmental changes during the plasma membrane remodeling.

3.5 TBTCP senses plasma membrane remodeling during phagocytosis

Based on these data, we further investigated the application of **TBTCP** in imaging macrophage phagocytosis. After staining the RAW 264.7 cells with **TBTCP**, about 10^8 CFU/mL ethanol-fixed Gram-negative bacteria *Escherichia coli* (*E. coli*) labeled with TPE-2BA, a blue-emission bacteria-labelling probe, were added to the cells [47]. The phagocytic process was observed by the confocal microscope after the addition of bacteria for 5 min (Figure S9). Some bacteria were found inside the RAW 264.7 cells, while some others were engulfed by the RAW 264.7 cells (Figure S10). These results clearly showed that macrophages could reach and interact with bacteria in a short period of time [48]. Then we tested changes in the fluorescence lifetime of **TBTCP** under the same conditions as the previous experiment but with unlabeled bacteria. The mean fluorescence lifetime of **TBTCP** in the plasma membrane of macrophages was about 3.543 ns in RAW 264.7 cells (Figure 4a and Figure S11). Its fluorescence lifetime decreased rapidly to 3.385 ns after incubated with the *E. coli* cultures. Similar results were obtained when Gram-positive bacteria such as *Bacillus subtilis* (*B. subtilis*, Figure S12) and *Staphylococcus epidermidis* (*S. epidermidis*, Figure S13) were used in the experiments. In comparison, the addition of bacteria cannot induce the fluorescence signal changes of HeLa cells, a type of non-professional phagocytes, which lack the phagocytic capacity for microorganisms (Figure 4b and Figure S14). This suggested that the fluorescence lifetime changes of **TBTCP** are associated with phagocytic activities in professional phagocytes. The comparable fluorescence lifetime of **TBTCP** in hypertonic conditions and during phagocytosis may suggest that the plasma membrane experiences similar membrane tension in both scenarios.

To understand what factors may induce the membrane status changes of macrophage in this process, we tested a few chemical and physical stimuli. It is reported that bacteria secrete toxins or proteins against phagocytes. Some exotoxins specifically target innate immune cells, which interfere with their phagocytic activities and alter the composition of the plasma membrane [49]. So we added the culture supernatant of *E. coli* to macrophages, stained the macrophages with **TBTCP** and imaged the cells under FLIM. However, there was no significant change in the fluorescence lifetime of **TBTCP** (Figure 5a and Figure S15). The lipopoly-

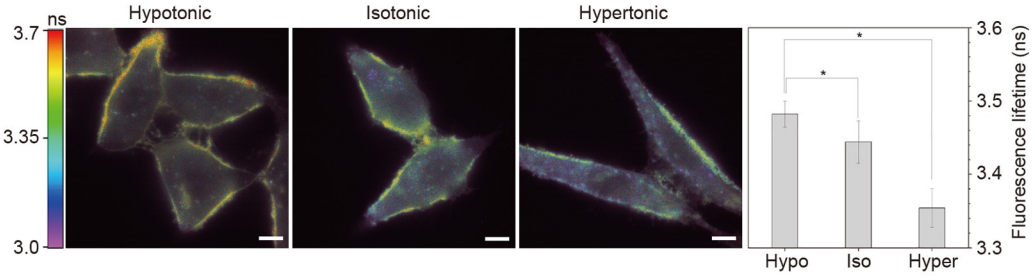

Figure 3 **TBTCP**-stained HeLa cells were incubated in solutions with different osmolarities. Fluorescence lifetime images were acquired by FLIM and the fluorescence lifetime of **TBTCP** was displayed in a pseudocolor format. The pseudocolor changes from orange to yellow and then green, along with the increase in the osmolarity revealed that **TBTCP** could sense the remodeling of the plasma membrane. The data are represented in mean ± SEM from at least three independent experiments. * $P < 0.05$. Scale bars: 10 μm (color online).

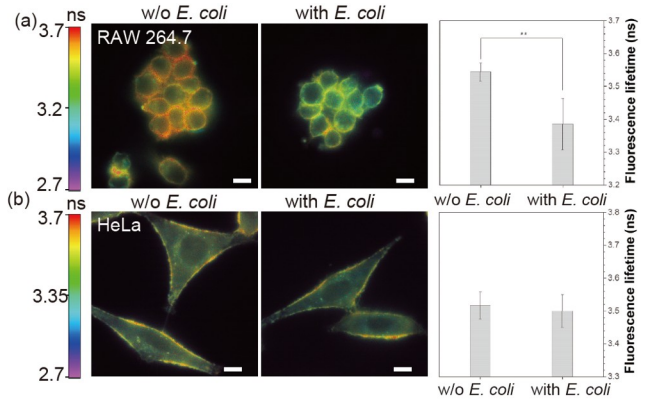

Figure 4 **TBTCP**-stained RAW 264.7 cells (a) and HeLa cells (b) were treated with or without (w/o) *E. coli*. The images of the fluorescence lifetime of **TBTCP** were acquired by FLIM and displayed in a pseudocolor format. Significant color changes from red to green, indicating a decrease in fluorescence lifetime, can be observed in the plasma membrane (a). The mean fluorescence lifetime of each group was measured and only RAW 264.7 cells decreased after treating with *E. coli*. The data are represented in mean ± SEM from at least three independent experiments. $^{**}P < 0.01$. Scale bars: 10 μm (color online).

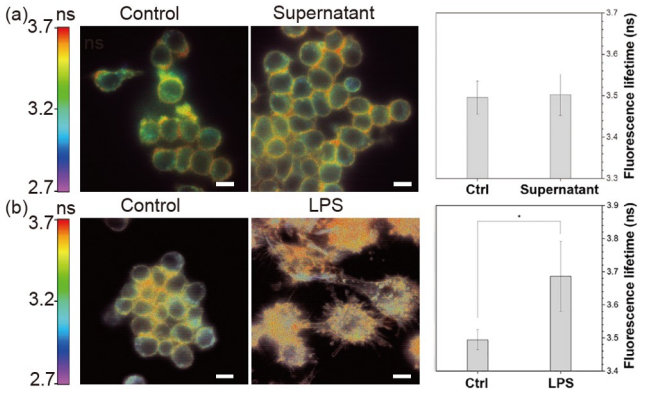

Figure 5 **TBTCP**-stained RAW 264.7 cells in the bacterial culture supernatant (a) or in pro-inflammatory responses (b). Fluorescence lifetime images were captured by FLIM and the mean fluorescence lifetime of each sample was measured. (a) RAW 264.7 cells were treated with the bacterial culture supernatant for 30 min. The mean fluorescence lifetime of **TBTCP** did not show a significant change compared to the control group. The data are represented in mean ± SEM from at least three independent experiments. (b) RAW 264.7 cells were first treated by LPS for 24 h and then stained with **TBTCP**. The mean fluorescence lifetime of **TBTCP** in the plasma membrane of LPS-treated group was higher than the control group. The data are represented in mean ± SEM from at least three independent experiments. $^{*}P < 0.05$. Scale bars: 10 μm (color online).

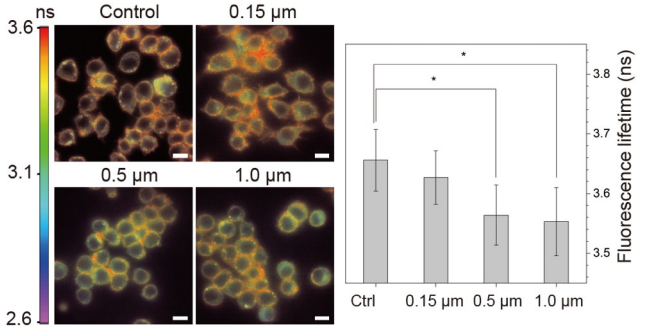

Figure 6 **TBTCP**-stained RAW 264.7 cells were exposed to different sizes of silica particles (1, 0.5 and 0.15 μm, respectively). Fluorescence lifetime images were captured by FLIM and the fluorescence lifetime of **TBTCP** in each sample was measured. The fluorescence lifetime of **TBTCP** decreased significantly when RAW 264.7 cells were incubated with 1-μm or 0.5-μm silica particles, but not with 0.15-μm silica particles. The data are represented in mean ± SEM from at least three independent experiments. $^{*}P < 0.05$. Scale bars: 10 μm (color online).

saccharide (LPS) is the outer membrane component of gram-negative bacteria that can induce macrophage activation [50]. It can stimulate macrophages to secrete pro-inflammatory cytokines, which lead to the inflammatory response [51]. These processes often cause alterations in the intracellular environment and the plasma membrane of macrophages [52]. To test whether LPS can also lead to the fluorescence lifetime changes of **TBTCP** in macrophage, we treated RAW 264.7 cells with 10 μg/mL LPS for 24 h [53]. Then, these cells were stained with **TBTCP** and imaged under FLIM (Figure 5b and Figure S16). Instead of showing a decreased fluorescence lifetime in the bacteria treated cells, **TBTCP** in the plasma membrane in the LPS-treated cells showed an increased mean fluorescence lifetime. The above results suggested that **TBTCP** can sense the alterations in the plasma membrane organization in the late pro-inflammatory response, which are distinguished from the early stages of macrophage phagocytosis.

Phagocytosis can be initiated not only by bacteria but also by dying cells or foreign particles of certain sizes [54]. Physical factors, such as particle shape and size, play important roles in inducing phagocytosis [54,55]. To study whether phagocytosis induced by changes in physical factors can be revealed by the **TBTCP** signal, **TBTCP**-stained RAW 264.7 cells were exposed to different-sized silica particles ranging from 0.15 to 1.0 μm. As shown in Figure 6 and Figure S17, the mean fluorescence lifetimes of **TBTCP** in the control cells (3.655 ns) and in the cells loaded with 0.15-μm silica particles (3.626 ns) were comparable. However, the mean fluorescence lifetime of **TBTCP** decreased to 3.563 and 3.552 ns when cells were loaded with larger-sized silica particles of 0.5 and 1.0 μm, respectively, indicating that only the large-sized silica particles (> 0.5 μm) can induce plasma membrane remodeling that can be sensed by **TBTCP**. Since the bacteria ranging from 0.5 to 5 μm or silica particles with such sizes are sufficient to decrease the fluorescence lifetime of **TBTCP**, it is likely that the decrease of **TBTCP** fluorescence lifetime is primarily due to the abrupt changes of the plasma membrane topography in macrophages during phagocytosis [54]. While for the uptake of small-sized silica particles, the cells may use other internalization machinery such as endocytosis [56]. The fluorescence lifetime of **TBTCP** maybe not be sensitive to small membrane invaginations. The uptake mechanisms of parti-

cles with different sizes can be revealed by the **TBTCP** signal and are supported by other studies [57].

4 Conclusions

In summary, an AIE-active plasma membrane-targeting fluorescent probe named **TBTCP** was rationally designed and synthesized. It was with NIR emission and high brightness. It had good biocompatibility and was able to selectively label the plasma membrane in different types of living cells with a short staining procedure, wash-free process, high signal-to-background ratio, and excellent photostability, which demonstrated the superiority over the commonly used commercially available fluorescent plasma membrane probes, such as CellMask™ Green and Vybrant DiO. When used in FLIM imaging, **TBTCP** showed a shorter fluorescence lifetime in the membrane of macrophage in the early stages of phagocytosis or in cells incubated in hypertonic solutions, which involves extensive remodeling of hyper-wrinkled cellular membranes. In contrast, hypotonic solutions or LPS-induced pro-inflammatory response caused cell swelling and increased the fluorescence lifetime of **TBTCP**. Silica nanoparticles with large-sizes (≥ 0.5 μm) but not the ones with the small-size can induce the phagocytosis of macrophages and can be revealed by the fluorescence lifetime changes of **TBTCP**. These data also suggested that though many factors may be involved in the fluorescence lifetime changes of **TBTCP** in phagocytic macrophages, the physical factor was one of the most important contributors. It offers the **TBTCP** a fast and sensitive response to the early stage of phagocytosis process and makes **TBTCP** a good probe for real-time imaging of phagocytosis. This article provides a valuable tool for phagocytosis imaging and other membrane-related studies. There are many environment-sensitive membrane-targeting fluorescent probes that have been employed in biosensing. For example, solvatochromic probes have been utilized in detecting the lipid order [58]; molecular rotors have been used in viscosity sensing [59,60] and flippers were developed to indicate the membrane tension [15,17]. In this study, we used an AIE membrane probe **TBTCP** for the phagocytosis imaging which may reveal a collective outcome of the complex changes in membrane physiology. We believe it will also inspire other researchers to explore more applications of AIE materials in this new direction.

Acknowledgements S. C. acknowledges the Start-up Funding from Ming Wai Lau Centre for Reparative Medicine, Karolinska Institutet. M-Y. W. thanks the National Natural Science Foundation of China (22177094, 21708030), the Applied Basic Research of Sichuan Province (2021YJ0397) and the Fundamental Research Funds for the Central University (2682021ZTPY039).

Funding note Open access funding provided by Karolinska Institute.

Conflict of interest The authors declare no conflict of interest.

Supporting information The supporting information is available online at http://chem.scichina.com and http://link.springer.com/journal/11426. The supporting materials are published as submitted, without typesetting or editing. The responsibility for scientific accuracy and content remains entirely with the authors

1 Stuart LM, Ezekowitz RA. *Nat Rev Immunol*, 2008, 8: 131–141
2 Cseresnyes Z, Hassan MIA, Dahse HM, Voigt K, Figge MT. *Front Microbiol*, 2020, 11: 1193
3 Rosales C, Uribe-Querol E. *Biomed Res Int*, 2017, 2017: 1–18
4 Arandjelovic S, Ravichandran KS. *Nat Immunol*, 2015, 16: 907–917
5 Gordon S. *Immunity*, 2016, 44: 463–475
6 Uribe-Querol E, Rosales C. *Front Immunol*, 2020, 11: 1066
7 Hampton MB, Vissers MCM, Winterbourn CC. *J Leukoc Biol*, 1994, 55: 147–152
8 Oki R, Kono M, Kubo K, Tojo A, Yamamoto K. *Kidney Int*, 2016, 90: 908
9 Wu MY, Leung JK, Liu L, Kam C, Chan KYK, Li RA, Feng S, Chen S. *Angew Chem Int Ed*, 2020, 59: 10327–10331
10 Lindner B, Burkard T, Schuler M. *Biotechniques*, 2020, 68: 245–250
11 Fernández A, Vendrell M. *Chem Soc Rev*, 2016, 45: 1182–1196
12 Becker W. *J Microsc*, 2012, 247: 119–136
13 Berezin MY, Achilefu S. *Chem Rev*, 2010, 110: 2641–2684
14 Suhling K, Hirvonen LM, Levitt JA, Chung PH, Tregidgo C, Le Marois A, Rusakov DA, Zheng K, Ameer-Beg S, Poland S, Coelho S, Henderson R, Krstajic N. *Med Photon*, 2015, 27: 3–40
15 Colom A, Derivery E, Soleimanpour S, Tomba C, Molin MD, Sakai N, González-Gaitán M, Matile S, Roux A. *Nat Chem*, 2018, 10: 1118–1125
16 Wu Z, Liu M, Liu Z, Tian Y. *J Am Chem Soc*, 2020, 142: 7532–7541
17 García-Calvo J, Maillard J, Fureraj I, Strakova K, Colom A, Mercier V, Roux A, Vauthey E, Sakai N, Fürstenberg A, Matile S. *J Am Chem Soc*, 2020, 142: 12034–12038
18 Yu L, Verwilst P, Shim I, Zhao YQ, Zhou Y, Kim JS. *CCS Chem*, 2021, 3: 2725–2739
19 Keshri P, Zhao B, Xie T, Bagheri Y, Chambers J, Sun Y, You M. *Angew Chem Int Ed*, 2021, 60: 15548–15555
20 Yang J, Chi Z, Zhu W, Tang BZ, Li Z. *Sci China Chem*, 2019, 62: 1090–1098
21 Guo Z, Yan C, Zhu WH. *Angew Chem Int Ed*, 2020, 59: 9812–9825
22 Cai X, Liu B. *Angew Chem Int Ed*, 2020, 59: 9868–9886
23 Li J, Wang J, Li H, Song N, Wang D, Tang BZ. *Chem Soc Rev*, 2020, 49: 1144–1172
24 Li J, Zhang Y, Wang P, Yu L, An J, Deng G, Sun Y, Seung Kim J. *Coord Chem Rev*, 2021, 427: 213559
25 Xu W, Wang D, Tang BZ. *Angew Chem Int Ed*, 2021, 60: 7476–7487
26 Bai H, He W, Chau JHC, Zheng Z, Kwok RTK, Lam JWY, Tang BZ.

Biomaterials, 2021, 268: 120598
27 Zhou Y, Hua J, Tang BZ, Tang Y. *Sci China Chem*, 2019, 62: 1312–1332
28 Gao H, Kam C, Chou TY, Wu MY, Zhao X, Chen S. *Nanoscale Horiz*, 2020, 5: 488–494
29 Kong M, Gu Y, Chai Y, Ke J, Liu Y, Xu X, Li Z, Feng W, Li F. *Sci China Chem*, 2021, 64: 974–984
30 Chen S, Hong Y, Zeng Y, Sun Q, Liu Y, Zhao E, Bai G, Qu J, Hao J, Tang BZ. *Chem Eur J*, 2015, 21: 4315–4320
31 Sarantis H, Grinstein S. *Methods Cell Bio*, 2012, 108: 429–444
32 Booth JW, Trimble WS, Grinstein S. *Semin Immunol*, 2001, 13: 357–364
33 Klymchenko AS, Kreder R. *Chem Biol*, 2014, 21: 97–113
34 Kijanka GS, Dimov IK, Burger R, Ducrée J. *Anal Chim Acta*, 2015, 872: 95–99
35 Kilin V, Glushonkov O, Herdly L, Klymchenko A, Richert L, Mely Y. *Biophysl J*, 2015, 108: 2521–2531
36 Collot M, Ashokkumar P, Anton H, Boutant E, Faklaris O, Galli T, Mély Y, Danglot L, Klymchenko AS. *Cell Chem Biol*, 2019, 26: 600–614
37 Liu C, Gao X, Yuan J, Zhang R. *TrAC Trends Anal Chem*, 2020, 133: 116092
38 Zhang K, Hu R, Wang Z, Tang BZ. *Mater Chem Front*, 2021, 5: 2724–2729
39 Sayed SM, Jia HR, Jiang YW, Zhu YX, Ma L, Yin F, Hussain I, Khan A, Ma Q, Wu FG, Lu X. *J Mater Chem B*, 2021, 9: 4303–4308
40 Wang D, Su H, Kwok RTK, Hu X, Zou H, Luo Q, Lee MMS, Xu W, Lam JWY, Tang BZ. *Chem Sci*, 2018, 9: 3685–3693
41 Wu MY, Wong AYH, Leung JK, Kam C, Wu KLK, Chan YS, Liu K, Ip NY, Chen S. *Proc Natl Acad Sci USA*, 2021, 118: e2106143118
42 Shi L, Liu YH, Li K, Sharma A, Yu KK, Ji MS, Li LL, Zhou Q, Zhang H, Kim JS, Yu XQ. *Angew Chem Int Ed*, 2020, 59: 9962–9966
43 Zhang Y, Wang Q, Zhu Z, Zhao W, Yan C, Liu Z, Liu M, Zhao X, Tian H, Zhu WH. *CCS Chem*, 2021, 3: 1800–1813
44 Zhang X, Wang C, Jin L, Han Z, Xiao Y. *ACS Appl Mater Interfaces*, 2014, 6: 12372–12379
45 Luo X, Li J, Zhao J, Gu L, Qian X, Yang Y. *Chin Chem Lett*, 2019, 30: 839–846
46 Martínez-Abadía M, Giménez R, Ros MB. *Adv Mater*, 2018, 30: 1704161
47 Zhao E, Hong Y, Chen S, Leung CWT, Chan CYK, Kwok RTK, Lam JWY, Tang BZ. *Adv Healthcare Mater*, 2014, 3: 88–96
48 Yeo JC, Wall AA, Stow JL, Hamilton NA. *Bio-techniques*, 2013, 55: 115–124
49 Vögele M, Bhaskara RM, Mulvihill E, van Pee K, Yildiz Ö, Kühlbrandt W, Müller DJ, Hummer G. *Proc Natl Acad Sci USA*, 2019, 116: 13352–13357
50 Ngkelo A, Meja K, Yeadon M, Adcock I, Kirkham PA. *J Inflamm*, 2012, 9: 2–8
51 Galli G, Saleh M. *Front Cell Infect Microbiol*, 2021, 10: 1
52 Williams LM, Ridley AJ. *J Immunol*, 2000, 164: 2028–2036
53 Meng F, Lowell CA. *J Exp Med*, 1997, 185: 1661–1670
54 Baranov MV, Kumar M, Sacanna S, Thutupalli S, van den Bogaart G. *Front Immunol*, 2021, 11: 1–23
55 Richards DM, Endres RG. *Proc Natl Acad Sci USA*, 2016, 113: 6113–6118
56 Doherty GJ, McMahon HT. *Annu Rev Biochem*, 2009, 78: 857–902
57 Conner SD, Schmid SL. *Nature*, 2003, 422: 37–44
58 Danylchuk DI, Jouard PH, Klymchenko AS. *J Am Chem Soc*, 2021, 143: 912–924
59 López-Duarte I, Vu TT, Izquierdo MA, Bull JA, Kuimova MK. *Chem Commun*, 2014, 50: 5282–5284
60 Páez-Pérez M, López-Duarte I, Vyšniauskas A, Brooks NJ, Kuimova MK. *Chem Sci*, 2021, 12: 2604–2613